Electron, Phonon and Thermoelectric Properties of Cu7PS6 Crystal Calculated at DFT Level

Bohdan Andriyevskyy (bohdan.andriyevskyy@tu.koszalin.pl)
Faculty of Electronics and Computer Sciences, Koszalin University of Technology, Śniadeckich str. 2, PL-75-453, Koszalin

Igor Barchiy
Inorganic Chemistry Department, Uzhhorod National University, Pidhirna str. 46, 88000 Uzhhorod

Ihor Studenyak
Inorganic Chemistry Department, Uzhhorod National University, Pidhirna str. 46, 88000 Uzhhorod

Andriy Kashuba
Department of General Physics, Lviv Polytechnic National University, Bandera str. 12, 79013 Lviv

Michał Piasecki
Institute of Physics, Jan Dlugosz University of Częstochowa, Armii Krajowej str. 13/15, Czestochowa

Research Article

Keywords: semiconductors, band structure, electron effective mass, electric conductivity, thermal conductivity, thermoelectric properties

Posted Date: July 21st, 2021

DOI: https://doi.org/10.21203/rs.3.rs-730770/v1

Electron, phonon and thermoelectric properties of Cu_7PS_6 crystal calculated at DFT level

B. Andriyevsky [a*], I. E. Barchiy [b], I. P. Studenyak [b], A. I. Kashuba [c], and M. Piasecki [d#]

[a] Faculty of Electronics and Computer Sciences, Koszalin University of Technology, Śniadeckich str. 2, PL-75-453, Koszalin, Poland
[b] Inorganic Chemistry Department, Uzhhorod National University, Pidhirna str. 46, 88000 Uzhhorod, Ukraine
[c] Department of General Physics, Lviv Polytechnic National University, Bandera str. 12, 79013 Lviv, Ukraine
[d] Institute of Physics, Jan Dlugosz University of Częstochowa, Armii Krajowej str. 13/15, Czestochowa, Poland

Abstract

The promising class of the environment-friendly thermoelectrics is the copper-based argyrodite-type ion-conducting crystals exhibiting just extraordinary low thermal conductivity below the glass limit associated with the molten copper sublattice leading to a softening of phonon modes. To explain why the argyrodite structure containing copper ions favors the low thermal conductivity, we have utilized the *ab initio* calculations of the electron, phonon, and thermoelectric properties of Cu_7PS_6 crystal in the framework of the density functional and Boltzmann transport theories. To obtain the reliable thermoelectric properties of Cu_7PS_6, we take into account the dependence of the electron effective mass m^* on the redundant carrier concentration n. We propose to use the Burstein-Moss effect for the calculation of the electron effective mass m^* of a semiconductor. We have found the strong nonlinear character of copper atom vibrations in Cu_7PS_6 which exceeds substantially the similar values for phosphorous and sulfur atoms. The large vibration nonlinearity of the copper atoms found in Cu_7PS_6 explains the diffusion-like heat transfer and the relatively low coefficient of the lattice thermal conductivity (κ = 0.7 W/(m·K)), which is favorable to achieve the large thermoelectric figure of merit.

Keywords: semiconductors, band structure, electron effective mass, electric conductivity, thermal conductivity, thermoelectric properties

1 Introduction

Cu_7PS_6 compound belongs to the argyrodite-type solid electrolytes [1]. At low temperatures the α-modification of the crystal belongs to the orthorhombic space groups $Pmn2_1$ (no. 31) ($T \le 213$ K) and $Pna2_1$ (no. 33) ($T \le 173$ K) [2]. At room temperature, the crystal structure of Cu_7PS_6 belongs to the cubic space group $P2_13$ (No. 198) with lattice parameter a = 0.96706 nm and four formula units per unit cell (Z = 4), which is identical to the structure of β-Cu_7PSe_6 [3]. The known solid electrolyte properties of Cu_7PSe_6 are due to the huge structural disorder of copper atoms/ions [4]. It was found that high room temperature total conductivity of Cu_7PSe_6, σ = 0.4 S/cm, is about 90% due to the electronic component of conductivity [4, 5]. The electric conductivity of Cu_7PS_6 in the temperature range 296 - 351 K was measured to be in the range $2\cdot10^{-5}$ - $5\cdot10^{-5}$ S/cm [3] that is much smaller than that in Cu_7PSe_6 [6]. Due to the same crystal structure of Cu_7PSe_6 and Cu_7PS_6 mentioned above the high structural disorder of copper atoms is expected in Cu_7PS_6, similarly like in Cu_7PSe_6 [4].

Recently, the effect of isovalent S^{2-} substitution for Se^{2-} in Cu_7PSe_6 on the crystal structure of the solid solution $Cu_7P(Se_{1-x}S_x)_6$ has been studied [7]. It was confirmed that the crystal structure of β-Cu_7PSe_6 transforms to the face-centered high-temperature γ-modification ($F\bar{4}3m$) above 320 K and the promising thermoelectric and ion conducting properties are observed only in this latter modification, where the cations are mobile, so the coper ion diffusion takes place. The similar transition for the homologous Cu_7PS_6 occurs at 510 K. One of the main results of this study is the anion ordering due to site preference of the sulfide ions. This leads to a stabilization of the high-temperature structure of $Cu_7P(Se_{1-x}S_x)_6$ even at lower temperatures. Thus, the isovalent substitution Se^{2-} by S^{2-} in $Cu_7P(Se_{1-x}S_x)_6$ allows the stabilization of the polymorph (γ-modification) with the most promising properties. This conclusion agrees with results of the previous study of the conductivity of solid solution $Cu_7P(Se_{1-x}S_x)_6$, where the phase transition from the primitive cubic structure $P2_13$ to the face-centered one $F\bar{4}3m$ was detected already at room temperature for the sulfur contents $x \ge 0.08$ [6].

Thus, the face-centered symmetry $F\bar{4}3m$, realized in Cu_7PS_6 and Cu_7PSe_6 crystals and their solid solution, is associated with the temperature-dependent copper ion diffusion, which introduces the structural

Corresponding authors: bohdan.andriyevskyy@tu.koszalin.pl [*], m.piasecki@ujd.edu.pl [#]
E-mail addresses: i_barchiy@ukr.net (I. E. Barchiy), studenyak@dr.com (I. P. Studenyak), andriykashuba07@gmail.com (A. I. Kashuba)

disorder or leads to amorphization. This amorphization causes the coefficient of thermal conductivity lowering and as a consequence increases the thermoelectric figure of merit. On the other hand, the copper ion diffusion in the crystal creates in fact the copper vacancies, which lead to the appearance of the electron donor states in the band structure. In turn, these electron states may increase electric conductivity, which also improves the material's thermoelectric characteristics. Thus, one may expect the increased ion- and electron-conducting properties among the representatives of $Cu_7P(Se_{1-x}S_x)_6$, which may induce advanced thermoelectric and solid electrolyte properties. That is why the theoretical study of the electron and phonon properties of Cu_7PS_6 and Cu_7PSe_6 crystals and their solid solutions $Cu_7P(Se_{1-x}S_x)_6$ is a promising task, solving of which may deliver more information on how to improve the solid electrolyte and thermoelectric properties of materials by appropriate selection of the chemical composition.

The most important electronic characteristics of a crystal for their thermoelectric and photovoltaic applications are the band gap E_g, the effective electron mass m^*, the carrier relaxation time τ, Sebeck coefficient α, and the coefficients of electric (σ) and thermal (κ) conductivities [8]. The ability to determine these characteristics for certain material compositions by using the theoretical methods is promising for the prediction of the main thermoelectric and photovoltaic characteristics (without having them synthesize) and evaluation of their possible practical applications. In the present study, we develop the consistent and complex methods to determine the mentioned above material constants by calculations within the density functional and Boltzmann transport theories. To illustrate the effectiveness of our approach, the proposed methods have been employed for Cu_7PS_6 crystal and the obtained results have been compared with experimental data. We intentionally have chosen this crystal out of other contents of $Cu_7P(Se_{1-x}S_x)_6$ solid solutions, because, Cu_7PS_6 possesses the relatively large energy gap, $E_g \approx 2$ eV, among other representatives of the group $Cu_7P(Se_{1-x}S_x)_6$, that is suitable for the study of the influence the extrinsic carriers on the electronic and thermoelectric properties of $Cu_7P(Se_{1-x}S_x)_6$ solid solutions. Further, having good consistency of our calculations with the available experimental data for Cu_7PS_6, in the next stage of our work, we intend to extend our calculations to a wide group of the argyrodite-type solid solutions to determine the chemical composition-structure-properties relations useful for finding the most effective thermoelectric material among this group.

2 Results and discussion

2.1. Electron band structure and related thermoelectric properties of Cu_7PS_6

The value of the energy gap E_g =0.83 eV obtained using the ordinary DFT approach (Fig. 1a) is more than twice smaller than the experimental one, E_g = 2.02 eV [9, 10]. The thermoelectric properties of Cu_7PS_6 calculated using the energy gaps E_g =0.83 eV and E_g = 2.02 eV have been found to be almost the same for different temperatures in the range $T < 500$ K, and therefore may be related to the extrinsic electrons in Cu_7PS_6. The mentioned above underestimation of the calculated energy gap E_g may be corrected using for example the DFT+U approach [11, 12], Heyd-Scuseria-Ernzerhof hybrid functional (HSE06) [13], or modified Becke-Johnson exchange potential with L(S)DA correlation [14, 15]. We used the HSE06 functional and the modified Becke-Johnson exchange potential (mBJ) and have obtained the calculated energy gap E_g close to the experimental one, E_g = 2.02 eV [9, 10].

The thermoelectric properties of the heavy degenerated wide energy gap semiconductors are determined mainly by the extrinsic charge carrier concentration in the conduction (*n*-type carriers) or valence (*p*-type carriers) bands and the energy gap value E_g = 2.0 eV of Cu_7PS_6, should not influence substantially these properties at the temperatures not much higher than the ambient one. Taking the later remark into account, we present the thermoelectric properties of Cu_7PS_6 calculated by the BoltzTrap2 code [16, 17] using the results of the ordinary DFT band structure calculations performed by VASP code [18-23] with opt-B86b exchange-and-correlation functional [24] and PAW-PBE pseudopotentials [23] and applying the scissor factor s = 2.0 corresponding to the energy gap E_g = 2.0 eV [9, 10].

The highest valence bands of the crystal Cu_7PS_6 in the range 0 – -3.0 eV are relatively flat (Fig. 1a). The highest valence band dispersion is observed at the points Γ and R of the Brillouin zone (Fig. 1a). The bottom conduction bands, located in the energy range of 0.83 eV - 5 eV, are characterized by the relatively large electron wave vector dispersion of energy $E(k)$ in comparison to the top valence bands. This means that the electron effective masses $m^* = \hbar^2/(d^2E/dk^2)$, as one of the main characteristic of semiconductors, for the bottom conduction bands are substantially smaller than the similar values for the top valence bands.

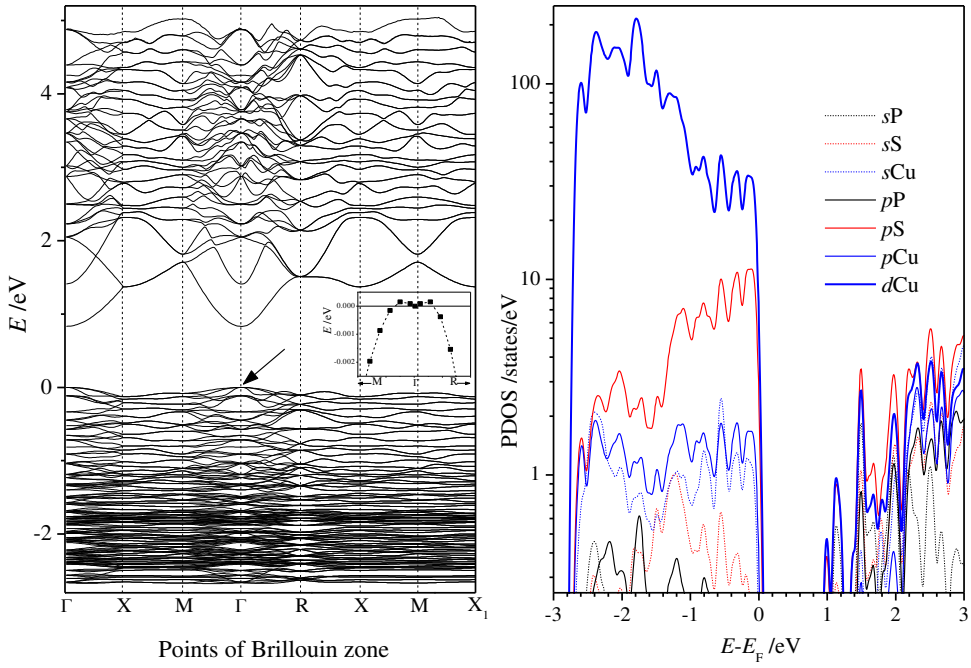

(a) (b)

Fig. 1. Band structure (a) and partial density of states (b) of Cu_7PS_6 for the symmetry space group no. 198 at the points Γ - 000, X – 010, M – ½½0, R - ½½½, X1 – 100 of BZ. The highest energy of the top valence band is placed at E = 0 eV. In inset, the enlarge $E(k)$ dependence of the top valence band v236 in the vicinity of Γ-point, shown by arrow

In view of the electric and thermoelectric properties of a material, the most significant energy ranges of the corresponding band structure are those neighboring to the energy gap E_g. The top valence and bottom conduction bands of the crystal in the range -3 eV - 3 eV are formed mainly by the *d*-electrons of copper and *p*-electrons of sulfur (Fig. 1b). This mainly is caused by the highest relative content of copper and sulfur atoms in Cu_7PS_6. The smallest PDOS of phosphorous is explained by the smaller its content in the formula unit Cu_7PS_6. The band structure is characterized by the relatively high hybridization of electronic states in the energy ranges close to the energy gap E_g, which manifests itself in the similar PDOS maxima in the range of the top valence and bottom conduction bands (Fig. 1b). Thus the bonding electrons of the most numerous atoms copper and sulfur form mainly the electronic states, which may be relevant to the electron conductivity of Cu_7PS_6.

The effective masses of electrons m^*_e and holes m^*_h are essential parameters characterizing the mobility of electric charges in semiconductor and substantially influence the thermoelectric and photoelectric properties [25]. The effective masses of electrons and holes in Cu_7PS_6 have been calculated by utilizing the Effective Mass Calculator [26] and by using the Burstein–Moss effect. In the later case, the excess charge carriers (electrons or holes), associated with doping of semiconductor, cause the energy gap increasing [27, 28]. The energy gap increase ΔE_g, caused by the excess electrons, is equal to the Fermi energy change $\Delta E_F = \Delta E_g$ depending on the carrier concentration n and the effective electron mass m^* in the conduction band,

$$\Delta E_F = \frac{h^2}{8\pi^2 m^*}\left(3\pi^2 n\right)^{2/3}, \qquad (1)$$

where h is Planck's constant. The energy gap increase ΔE_g may be caused by the excess or lack of electrons in the crystal unit cell. On the basis of the measured or calculated value $\Delta E_g = \Delta E_F$ and using the relation (1) one can calculate the effective electron or hole masses, m^*_e or m^*_h, corresponding to the ranges of conduction (c) or valence (v) bands. In the present study, the energy gap increase $\Delta E_g = \Delta E_F$, caused by the excess electron concentration n, was simulated computationally and taken as the Fermi energy shift $\Delta E_F = E_F - E_{cbm}$, where E_F is the Fermi energy of the *n*-type semiconductors studied and E_{cbm} is the energy of the conduction band minimum E_{cbm} of the nominal material. Similarly, in the case of the hole conductivity, the value of ΔE_F was taken as the Fermi energy shift $\Delta E_F = E_F - E_{vbm}$, where E_{vbm} is the energy of the valence band maximum of the nominal semiconductor. The corresponding calculations have been performed for the excess electron and hole

concentrations n_e and n_h of the order of 10^{20} cm^{-3}, which corresponds to the excess (n_e) or lack (n_h) of not more than four electrons in the supercell 2×2×2 of Cu_7PS_6 containing 448 atoms. Due to the additional test calculations performed, we have revealed that these concentrations of the redundant electrons and holes do not change the energy dependence of density of states in the whole range of valence and conduction bands.

The calculated dependence of the Fermi level shift ΔE_F on the excess electron/hole concentration $n^{2/3}$ reveals a linear behavior for the holes in accordance with the relation (1) and with the effective mass $m_h^* = -6.15\ m_e$ (range of positive values of $n^{2/3}$ in Fig. 2a). However, in the range of excess electrons, the linear dependence does not fulfill in the whole range of the negative $n^{2/3}$ values (Fig. 2a). For the carrier concentrations n, not larger than the absolute value $2.8\cdot10^{20}$ cm^{-3} ($n^{2/3} = 4.3\cdot10^{13}$ cm^{-2}), the linear dependence is observed and the corresponding electron effective mass is relatively small, $m_e^* = 0.581\ m_e$ (Fig. 2a). This value is very close to that obtained for the first conduction band c237 at Γ-point of BZ by using Electron Mass Calculator, $m_e^* = 0.59\ m_e$ (SI-Table 1). For the carrier concentrations n, larger than the absolute value $2.8\cdot10^{20}$ cm^{-3} ($n^{2/3} = 4.3\cdot10^{13}$ cm^{-2}), the values of Fermi level shift ΔE_F are much smaller of those satisfying the linear dependence ΔE_F vs. $n^{2/3}$ in the whole range of $n^{2/3}$ change presented in Fig. 2a. This means that for the excess electron concentrations n, larger than the absolute value $2.8\cdot10^{20}$ cm^{-3}, the corresponding electron effective masses become substantially larger and may be comparable by absolute value with the effective mass for holes (Fig. 2a). This result is generally in agreement with the band structure view of the conduction bands of Cu_7PS_6, where the decrease of the band dispersion d^2E/dk^2 is clear visible at an increase of energy (Fig. 1a), which corresponds to the increase of the electron effective mass m^* (there is no such clear change of the band dispersion d^2E/dk^2 in the range of the top group of valence bands (Fig. 1a), that is in agreement with the constant value of the effective mass $m^* = -6.15\ m_e$ derived from Fig. 2a. The solid line in the range of negative values of n in Fig. 2b is obtained by the nonlinear fitting of the dependence $\Delta E_F(n^{2/3})$ in the corresponding range of $n^{2/3}$ (Fig. 2a).

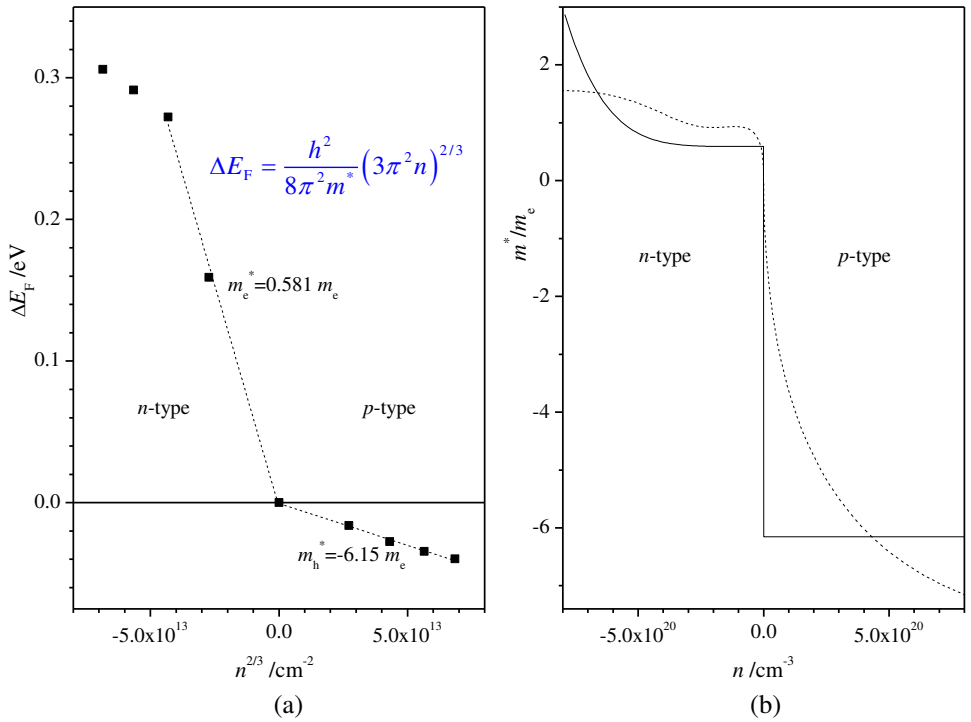

Fig. 2. (a) Fermi level shift ΔE_F as function of the excess electron/hole concentration $n^{2/3}$ for Cu_7PS_6. Negative values of $n^{2/3}$ correspond to the excess electrons (n-type Cu_7PS_6) and positive ones to the excess holes (p-type Cu_7PS_6). Signs of the effective masses $m^* = 0.581\ m_e$ and $m^* = -6.15\ m_e$ are chosen to be compatible with the effective mass definition $m^* = \hbar^2/(d^2E/dk^2)$; (b) Effective electron mass m^*/m_e as function of the excess electron/hole concentration n calculated from BoltzTraP2 Seebeck coefficient α and relation (1) (dashed line) and from the data of Fig. 2a (solid line)

The analysis of the electron/hole effective mass of Cu_7PS_6 presented above indicates that, in the range of the excess electron concentration n between approximately $-4\cdot10^{20}$ cm^{-3} and $4\cdot10^{20}$ cm^{-3}, the effective mass of the conduction electrons is approximately one order of magnitude smaller than the similar value for the holes. Thus, one may expect the corresponding differences in the physical values of Cu_7PS_6 depending on the effective electron mass.

Several thermoelectric properties of Cu_7PS_6 have been calculated in the framework of DFT using the VASP and BoltzTraP2 codes. One of the main thermoelectric parameters is the Seebeck coefficient (α), which is proportional to the charge carrier effective mass m^*, temperature T, and the inverse charge carrier density $n^{-2/3}$ [29],

$$\alpha = \frac{2k_B^2}{3eh^2} m^* T \left(\frac{\pi}{3n}\right)^{\frac{2}{3}} . \qquad (2)$$

Here, k_B is the Boltzmann's constant, e is the electron charge, h is Planck's constant. Thus, a large Seebeck coefficient is expected in material possessing high effective mass and low carrier concentration. Having calculated the Seebeck coefficient of Cu_7PS_6 by using the corresponding calculations of VASP and BoltzTraP2 (Fig. 3) one has possibility to calculate the effective mass m^* from the relation (2) (see Fig. 2b). Thus calculated effective mass m^* is comparable with that obtained by the method utilizing the Burstein-Moss effect in the range of the n-type carriers (excess of valence electrons) (Fig. 2b). A similar comparison however is not so good for the p-type carriers (lack of valence electrons) (Fig. 2b). For the range of the positive carrier concentrations n, the monotonous dependence the corresponding effective mass $m^*(n)$ with decreasing absolute value of $|m^*|$ at decreasing n has been obtained when using the relation (2) (Fig. 2b). This result does not agree with the relatively large absolute value of the hole effective mass $|m_h^*| = 6.15\ m_e$, expected on the basis of the low valence band energy dispersion d^2E/dk^2 of Cu_7PS_6 mentioned earlier. So, the values m^*, in the range of the relatively small carrier concentrations $|n| < 5\cdot10^{19}$ cm^{-3}, derived from the classical Boltzmann theory by applying the relation (2) (dashed line in Fig. 2b), are not reasonable.

According to the relation of the effective masses $m_h^* > m_e^*$ mentioned above (Fig. 2b), the determined Seebeck coefficient α is larger for the p-type carriers of Cu_7PS_6, in comparison to the n-type one (Fig. 3a). The decrease of the absolute value of Seebeck coefficient α is observed when the carrier concentration n increases. For every carrier concentration n the absolute value of Seebeck coefficient α increases with the increase in temperature (Fig. 3a). These features are in agreement with the relation (2).

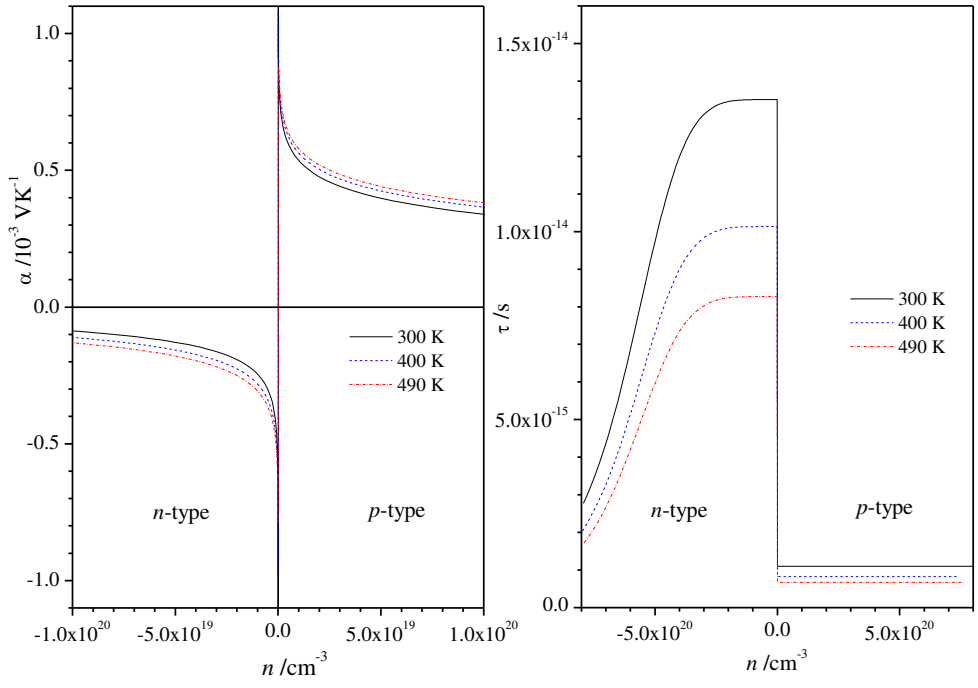

Fig. 3. Dependences of (a) Seebeck coefficient α and (b) carrier relaxation time τ on carrier concentration n for Cu_7PS_6 at the temperatures 300 K, 400 K, and 490 K

The specific electric conductivity σ of material is one of the main parameters responsible for thermo-electrical properties. The BoltzTrap2 code gives possibility to determine the value σ/τ, where τ is the carrier relaxation time (many semiconductors are characterized by the relaxation time of 10^{-13} - 10^{-14} s [30 - 32]). Thus, to get the specific conductivity σ from the calculated value σ/τ, it is necessary to obtain the τ independently. This value has been calculated using the known relation between the carrier relaxation time τ and the carrier mobility μ,

$$\tau = \frac{m^*}{e}\mu \ . \tag{3}$$

In turn, the carrier mobility μ has been calculated in the framework of the Deformation Potential Theory using the relation, [33, 34],

$$\mu_j = \frac{e\hbar^3 C_j}{k_B T m_j^* m_d \left(E_j^2\right)} \ , \quad j = x, y \tag{4}$$

where m_j^* is the carrier effective mass in direction of motion j and $m_d = \sqrt{m_x^* m_y^*}$ represents the average of effective masses along x- and y-direction. The term E_j designates the deformation potential constant of holes and electrons in the valence band maximum and conduction band minimum, respectively, along the transport direction. It is defined as $E_j = \Delta E^{(band)}_j/\varepsilon$, where $\Delta E^{(band)}_j$ represents the energy change of the j-th band caused by cell deformation (elongation and compression), and ε denotes the applied strain, which is given by $\varepsilon = \Delta a/a$. Here a and Δa are the optimized lattice constant and the change of a along the transport direction, respectively [33, 34]. The DPT approach was extensively used to calculate the intrinsic mobility in semiconductors [8, 33, 34,].

The elastic constants C_j (4) along the direction j are obtained by the parabolic fitting of the equation $(E - E_0)/A_0 = C_j\varepsilon^2/2$, where E is the calculated energy of the crystal unit cell under strain. In the present study, the values E_0 and A_0 are the equilibrium energy and the characteristic area, $A_0 = a^2$, for the cubic unit cell of Cu_7PS_6.

Thus, calculated dependence of the relaxation time on the carrier concentration $\tau(n)$ is presented in Fig. 3b. This concentration dependence is determined by the corresponding dependence of the electron effective mass $m^*(n)$ (Fig. 2b). Other values in the formula (4), i.e. C_j and E_j, have been kept constant in the present study.

Having calculated the relaxation time τ, we have obtained the specific conductivity σ (Fig. 4a) and, afterward, the power factor $PF = \alpha^2\sigma$ (Fig. 4b) using the results of BoltzTrap2 calculations of Seebeck coefficient α. The monotonous increase of specific conductivity σ with an increase of carrier concentration n is expected in the whole range of n up to $n = 1\cdot10^{20}$ cm^{-3} for both types of charge carriers (Fig. 4a). Here, the n-type conductivity of Cu_7PS_6 is about two orders of magnitude larger than the p-type one. Similar monotonous increase takes place for the concentration dependence of the power factor PF for the p-type carriers (Fig. 4b). The characteristic maxima of concentration dependences of the power factor PF for different temperatures take place for the n-type carriers (Fig. 4b). The maxima observed in Fig. 4b are caused by the opposite behaviors of the concentration dependences of the Seebeck coefficient $\alpha(n)$ (Fig. 3a) and the specific conductivity $\sigma(n)$ (Fig. 4a). The relation of power factors for n- and p-type carriers is about 5 and is not so large as that mentioned above for the corresponding conductivities. This is caused by the larger Seebeck coefficient for p-type carriers than that for n-type one. The calculations have revealed that for the carrier concentration $n > 2.6\cdot10^{19}$ cm^{-3} the characters of temperature dependences of the power factor PF in the ranges of n- and p-type carriers are opposite (Fig. 4b). This is caused by the larger influence of the value α^2 than of the value σ into the power factor $PF = \alpha^2\sigma$ for the carrier concentration $n > 2.6\cdot10^{19}$ cm^{-3}.

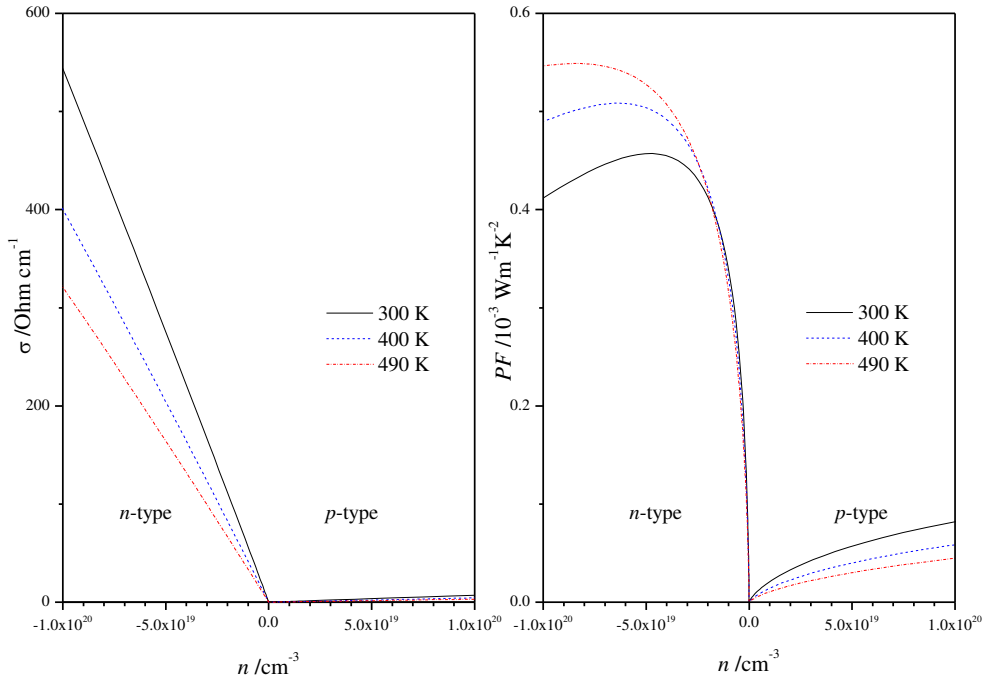

(a) (b)

Fig. 4. Dependences of (a) electric conductivity σ, (b) power factor *PF*, and figure of merit *ZT* on carrier concentration *n* for Cu_7PS_6 at the temperatures 300 K, 400 K, and 490 K

To obtain the value of the thermoelectric figure of merit ZT of material,

$$ZT = \frac{\alpha^2 \sigma T}{\kappa} \quad , \tag{5}$$

one has to know the coefficient of thermal conductivity κ. The later value is a sum of the corresponding electron and lattice (phonon) components, $\kappa = \kappa_e + \kappa_{ph}$. The coefficient of electron thermal conductivity κ_e of Cu_7PS_6 has been determined from the quotient κ_e/τ, obtained by the BoltzTrap2 code, and the previously calculated carrier relaxation time τ (Fig. 3a). It is seen from Fig. 5a, that the largest coefficient κ_e = 0.35 W/(m·K) may be achieved only for the degenerated semiconductor of the relatively high excess electron concentration $n = 1 \cdot 10^{20}$ cm^{-3}. For the less degenerated Cu_7PS_6, $n = 1 \cdot 10^{19}$ cm^{-3}, the coefficient of electron thermal conductivity is one order of magnitude smaller, κ_e = 0.03 W/(m·K) (Fig. 5a). To predict the reliable figure of merit *ZT* of Cu_7PS_6 one has to use the total coefficient of thermal conductivity $\kappa = \kappa_e + \kappa_{ph}$. Thus, estimation of the coefficient of lattice thermal conductivity κ_{ph} is necessary to obtain the reliable value of the total coefficient of thermal conductivity κ and finally the figure of merit *ZT*.

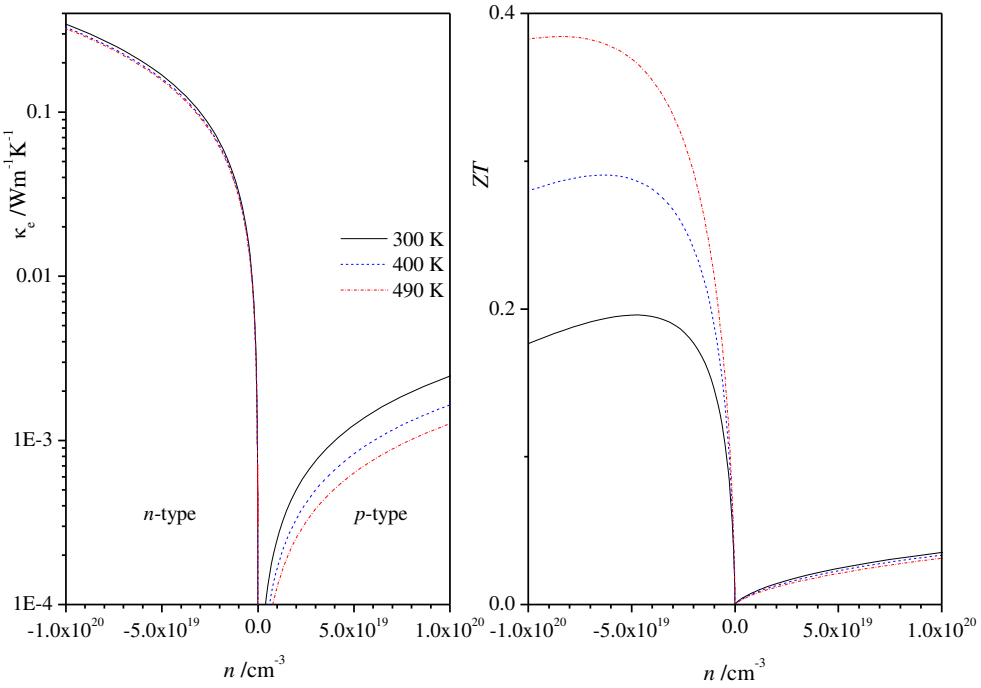

Fig. 5. Dependences of (a) coefficient of electron thermal conductivity κ_e and (b) figure of merit *ZT* on carrier concentration *n* for Cu_7PS_6 at the temperatures 300 K, 400 K, and 490 K. The values *ZT* correspond to the coefficient of thermal conductivity κ = 0.7 W/(m·K)

2.2. Lattice-based thermal conductivity of Cu_7PS_6

Two models of thermal conductivity in solids have been used to estimate the coefficient of the lattice thermal conductivity of Cu_7PS_6. The first one is phonon-based and the second one is diffusion-based [35]. The phonon-based model is implemented in the Phono3py code [36] and is usually applied to the crystalline solids of the high and moderate coefficient of thermal conductivity. In turn, the diffusion-based model of Allen and Feldman [37 - 39] is applied more successfully to the amorphous or polycrystalline materials possessing the relatively small coefficient of thermal conductivity. The Cu_7PS_6 crystal is close to the latter type of materials due to the weak bonding of copper atoms in the structure, similar to that found in Cu_7PSe_6 [4].

In the phonon based model, the coefficient of thermal conductivity is calculated by the relation,

$$\kappa_{ph}^{(1)} = \frac{1}{3} c v_g^2 \tau \ , \tag{6}$$

where *c* is the specific heat, v_g^2 is the phonon group velocity and τ is the phonon relaxation time. In the diffusion-based model, the maximum thermal conductivity is calculated by the relation,

$$\kappa_{ph}^{(2)} = \frac{n^{\frac{1}{3}} k_B}{\pi} \omega_{avg} \ , \tag{7}$$

where *n* is the number density of atoms, ω_{avg} is the averaged oscillator frequency, k_B is the Boltzmann constant [35]. In the present study, the averaged oscillator frequency ω_{avg} of Cu_7PS_6 has been obtained from the calculated vibration density of states obtained by using the lattice and molecular dynamics (SI-Fig. 1 and SI-Fig. 2).

The coefficient of lattice thermal conductivity $\kappa_{ph}^{(1)}$ of Cu_7PS_6 was calculated using the VASP and Phono3py codes [36, 40]. We have revealed that the coefficient $\kappa_{ph}^{(1)}$ of Cu_7PS_6 depends very much on the displacement amplitude of atoms. For the default displacement amplitude of 0.03 Å, the maximum value of $\kappa_{ph}^{(1)}$ is about 27 W/(m·K). Because the spring constant k_{Cu} of copper atoms in Cu_7PS_6 is about four times smaller than those for phosphorous and sulfur ones (see SI), the large displacement amplitude of 0.3 Å has also been used for calculation of the κ_{ph} coefficient using Phono3Py code. We have revealed that the $\kappa_{ph}^{(1)}$ coefficient of Cu_7PS_6 depends also on the *q*-points mesh of the inverse lattice used (Fig. 6). Thus, in the case of the displacement

amplitude of 0.3 Å and the *q*-points mesh of 6×6×6 the maximum value of $\kappa_{ph}^{(1)}$ is found to be about 7 $Wm^{-1}K^{-1}$ at room temperature (Fig. 6).

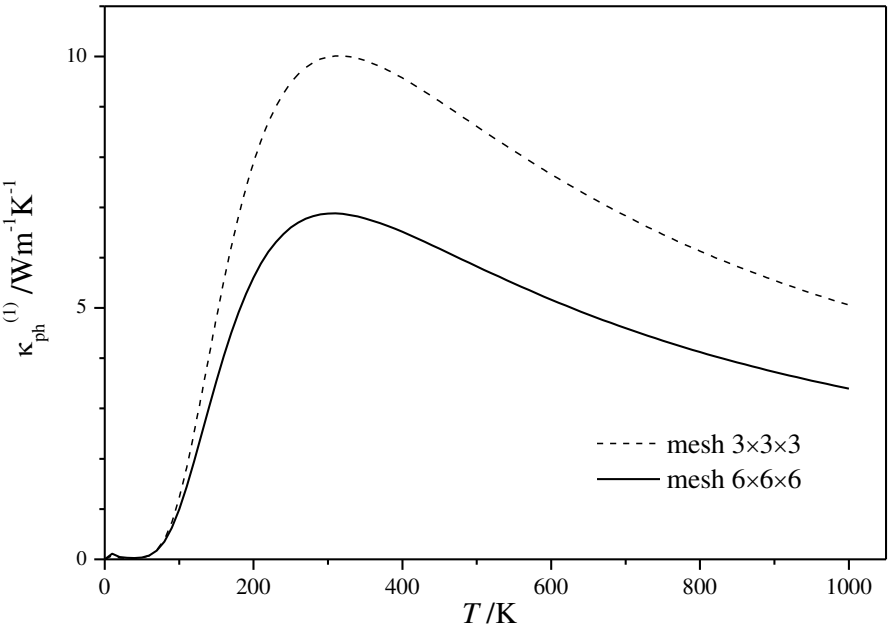

Fig. 6. Temperature dependences of lattice thermal conductivity coefficient $\kappa_{ph}^{(1)}$ of Cu_7PS_6 obtained using Phono3py with displacement amplitude of 0.3 Å and *q*-meshes of 3×3×3 (dashed line) and 6×6×6 (solid line)

Temperature dependence of the coefficient of thermal conductivity $\kappa_{ph}^{(2)}$ of Cu_7PS_6 calculated in the framework of the diffusion model, exploited by G. J. Snyder group [35], using the relation (7) and results of MD calculations are presented in Fig. 7. In the temperature range of 300 K - 800 K, the coefficient of thermal conductivity $\kappa_{ph}^{(2)}$ of Cu_7PS_6 remains almost constant, $\kappa_{ph}^{(2)}$ = 0.7 W/(m·K). The calculated value $\kappa_{ph}^{(2)}$ = 0.7 W/(m·K) for Cu_7PS_6 is of the same order of magnitude as the value $\kappa_{ph}^{(exp)} \approx 0.2 – 0.3$ $Wm^{-1}K^{-1}$ experimentally measured for the similar compound Cu_7PSe_6 [41]. That is why the value $\kappa_{ph}^{(2)}$ = 0.7 W/(m·K), obtained in the framework of the diffusion model of thermal conductivity [35], has been used for the calculation of the figure of merit *ZT* of Cu_7PS_6 (Fig. 5b). The coefficient of lattice thermal conductivity $\kappa_{ph}^{(2)}$ = 0.7 W/(m·K) is one order of magnitude smaller than the similar value $\kappa_{ph}^{(1)}$ = 7 W/(m·K) obtained by utilizing Phono3py code (Fig. 13). Using thus calculated value of the lattice thermal conductivity $\kappa_{ph}^{(2)}$ = 0.7 W/(m·K) of Cu_7PS_6 the corresponding calculated temperature dependence of the figure of merit *ZT* (Fig. 5b) is found to be comparable with the experimental temperature dependence of *ZT* for Cu_7PSe_6 [41].

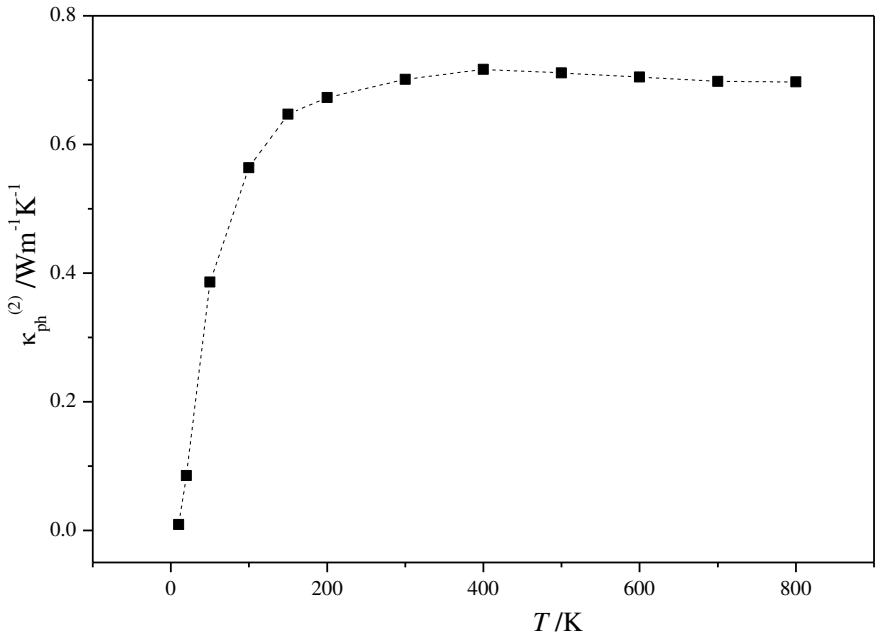

Fig. 7. Temperature dependence of lattice thermal conductivity coefficient $\kappa_{ph}^{(2)}$ of Cu_7PS_6 obtained by using the results of molecular dynamics calculations and relation (7)

3 Methods of calculations

Study of the electronic properties of Cu_7PS_6 crystals were performed in the framework of the density functional theory (DFT) using the VASP code [18 - 23] and PAW pseudopotentials [23]. In view of the relatively large conventional unit cell of the crystal ($a = b = c = 9.59$ Å, space group no. 198), the dispersion interactions (van der Waals) have been taken into account in the form of the opt-B86b functional [24].

Before the production calculations of the crystal studied, the total energy convergence tests were performed in relation to the cutoff energy of plane waves (E_{cutoff}) and k-points grid used. Finally, the cutoff energy $E_{cutoff} = 390$ eV and the k-points grids from 6×6×6 to 10×10×10 of the reciprocal lattice have been used, depending on the type of the calculation task.

To determine the thermoelectric properties (Seebeck coefficient, electron electrical conductivity per relaxation time, electron thermal conductivity per relaxation time and related thermoelectric values) the Boltzmann Transport Properties code (BoltzTraP2) was applied [16, 17]. BoltzTraP2 computes several properties related to the thermoelectric effect in materials within the rigid band approximation based on the semi-classical Boltzmann transport theory [42] with the density of electron states (DOS) only as the input. Therefore, before the calculations of thermoelectric properties using BoltzTraP2 code [17], the DFT calculations of the electronic band structure were performed using the VASP code.

The coefficient of lattice thermal conductivity $\kappa_{ph}^{(1)}$ of Cu_7PS_6 was calculated using the VASP and Phono3py codes [36, 40]. To obtain a reasonable value of κ_{ph} coefficient one generally should not use small unit cell [36]. Due to the relatively large unit cell dimensions of Cu_7PS_6 crystal ($a = b = c = 9.6$ Å) the supercell 1×1×1 has been used for the corresponding calculations. On the other hand, a use of the larger supercells together with dense k-point grid for this purpose may not be acceptable because of the huge amount of the necessary computational resources.

To obtain better insight into the phonon-associated effects in Cu_7PS_6 crystal the molecular dynamics calculations have been performed using the VASP code at different temperatures in the range of 20 – 800 K. The results of MD obtained were elaborated using the nMoldyn 3.0 code [43].

4 Conclusions

A comprehensive *ab initio* set of methods for determining the main thermoelectric material parameters has been proposed and has been applied to the Cu_7PS_6 crystal of the argyrodite-type structure. The relationship between the calculated electron and phonon properties, on the one hand, and thermoelectric properties, on the other hand,

is discussed. This relationship allow the prediction of the intentional changes in the chemical composition of the materials family $Cu_7P(S_{1-x}Se_x)_6$ to obtain the desired thermoelectric properties.

The Burstein-Moss effect is shown to be successfully utilized for the calculation of the electron effective mass dependence on the electric carrier concentration in Cu_7PS_6 crystal. A substantial dependence of the electron effective mass on the carrier concentration in Cu_7PS_6 was found for the excess electron concentration in the range $n > 3 \cdot 10^{20}$ cm^{-3}, which should be taken into account in the calculation of thermoelectric properties.

The relatively high temperature stimulated mobility of the copper atoms in comparison to the phosphorous and sulfur ones found in Cu_7PS_6 crystal justifies the applying of the diffusion-based model of thermal conductivity. In the framework of this model, the calculated coefficient of thermal conductivity of Cu_7PS_6, $\kappa^{(Cu7PS6)} \approx 0.7$ $Wm^{-1}K^{-1}$, is close to the experimental value for Cu_7PSe_6 crystal, $\kappa_{exp}^{(Cu7PSe6)} \approx 0.2 - 0.3$ $Wm^{-1}K^{-1}$, belonging to the same argyrodite-type structure.

The thermal conductivity properties of Cu_7PS_6 crystal have been determined using different approaches: (a) by the Boltzmann phonon transport theory (Phono3py code), (b) by the analysis of nonlinearities in the lattice and molecular dynamics, (c) by applying the random walk theory and using the quasi-particles transferring heat (diffusons). The most suitable approach, giving the coefficient of thermal conductivity of the real polycrystalline Cu_7PS_6 samples close to the corresponding experimental results, is the heat transfer mediated by diffusons. Using this approach, the calculated coefficient of the lattice thermal conductivity of Cu_7PS_6 at high-temperature limit $\kappa_{ph} = 0.7$ W/(m·K) is found to be of the same order of magnitude as the experimental one, $\kappa_{exp} \approx 0.2 - 0.3$ $Wm^{-1}K^{-1}$.

For the heavy doped *n*-type Cu_7PS_6 of about $1 \cdot 10^{19}$ - $1 \cdot 10^{20}$ cm^{-3}, the calculated values of the figure of merit *ZT* for the temperatures in the range 300 - 500 K are comparable with the corresponding experimental reference values for the similar compound Cu_7PSe_6.

We believe that the proposed method will be an effective tool in the search of perspective thermoelectric materials.

Acknowledgements

Computer calculations have been performed at ICM of Warsaw University, Poland (project No. GB81-13) and WCSS of Wrocław University of Technology, Poland (project No. 053).

References

[1] Kuhs, W. F.; Nitsche, R.; Scheunemann, K. The argyrodites – a new family of tetrahedrally close-packed structures. *Mater. Res. Bull.* **14**, 241–248 (1979).

[2] Gaudin, E.; Petricek, V.; Boucher, F.; Taulellec, F.; Evaina, M. Structures and phase transitions of the A_7PSe_6 (A = Ag, Cu) argyrodite-type ionic conductors. III. a-Cu_7PSe_6. *Acta Cryst.* **B56**, 972 - 979 (2000).

[3] Studenyak, I. P.; Izai, V. Yu.; Pogodin, A. I.; Kokhan, O. P.; Sidey, V. I.; Sabov, M. Yu.; Kežionis, A.; Šalkus, T.; Banys. Structural and electrical properties of argyroditetype Cu7PS6 crystals. J. *Lith. J. Phys.* **57**, 243–251 (2017).

[4] Beeken, R. B.; Driessen, C. R.; Hinaus, B. M.; Pawlisch, D. E. Electrical conductivity of Ag_7PSe_6 and Cu_7PSe_6. *Solid State Ionics* **179**, 1058–1060 (2008).

[5] Baumer, F., Nilges, T. *Z.* Phase segregation of polymorphic solid ion conducting Cu_7PSe_6 during thermoelectric experiments. *Anorg. Allg. Chem.* **644**, 1519-1524 (2018).

[6] Beeken, R. B.; Hinaus, B. M. The effect of sulfide substitution in the mixed conductor Cu_7PSe_6. *J. Phys. Chem. Solids* **72**, 1081–1084 (2011).

[7] Reissig, F.; Heep, B.; Panthöfer, M.; Wood, M.; Anand, S.; Snyder, G. J.; Tremel, W. Effect of anion substitution on the structural and transport properties of argyrodites $Cu_7PSe_{6-x}S_x$. *Dalton Trans.* **48**, 15822-15829 (2019).

[8] Vu, T.V.; Nguyen, C.V.; Phuc, H.V.; Lavrentyev, A.A.; Khyzhun, O.Y.; Hieu, N.V.; Obeid, M.M.; Rai, D.P.; Tong, H.D.; Hieu, N.N. Theoretical prediction of electronic, transport, optical, and thermoelectric properties of Janus monolayers In_2XO (X=S,Se,Te). *Phys. Rev. B* **103**, 085422 (2021).

[9] Studenyak, I. P.; Luchynets, M. M.; Pop, M. M.; Studenyak, V. I.; Pogodin, A. I.; Kokhan, O.P.; Grancic, B.; Kúš, P. Elastic properties of $CdTe_{1-x}Se_x$ (x = 1/16) solid solution: First principles study. *Semiconductor Physics, Quantum Electronics & Optoelectronics* (*SPQEO*), **22**, 347-352 (2019).

[10] Studenyak, I. P.; Luchynets, M. M.; Izai, V. Yu.; Pogodin, A. I.; Kokhan, O. P.; Azhniuk, M.; Zahn, D. R. T. Structural and optical properties of $(Cu_6PS_5Br)_{1-x}(Cu_7PS_6)_x$ mixed crystals. *J. Alloys Compounds* **782**, 586-591 (2019).

[11] Rohrbach, A.; Hafner, J.; Kresse, G. Electronic correlation effects in transition-metal sulfides. *J. Phys.: Condens. Matter* **15**, 979–996 (2003).

[12] Bengone, O.; Alouani, M.; Blöchl, P.; Hugel, J. Implementation of the projector augmented-wave LDA+U method: Application to the electronic structure of NiO. *Phys. Rev. B* **62**, 16392 (2000).

[13] Heyd, J.; Scuseria, G. E.; Ernzerhof, M. Hybrid functionals based on a screened Coulomb potential. *J. Chem. Phys.* **118**, 8207 (2003).

[14] Becke, A.D.; Johnson, E.R. A simple effective potential for exchange. *J. Chem. Phys.* **124**, 221101 (2006).

[15] Tran, F.; Blaha, P. Accurate band gaps of semiconductors and insulators with a semilocal exchange-correlation potential. *Phys. Rev. Lett.* **102**, 226401 (2009).

[16] Madsen, G. K. H.; Carrete, J.; Verstraete, M. J. BoltzTraP2, a program for interpolating band structures and calculating semi-classical transport coefficients. *Comput. Phys. Commun.* **231**, 140–145 (2018).

[17] Madsen, G. K. H.; Singh, D. J. BoltzTraP. A code for calculating band-structure dependent quantities. *Comput. Phys. Commun.* **175**, 67-71 (2006).

[18] Kresse, G.; Hafner, J. Ab initio molecular dynamics for liquid metals. *Phys. Rev. B* **47**, 558-561 (1993).

[19] Kresse, G.; Hafner, J. Ab initio molecular-dynamics simulation of the liquid-metal-amorphous-semiconductor transition in germanium. *Phys. Rev. B* **49**, 14251-14269 (1994).

[20] Kresse, G.; Furthmüller, J. Efficiency of ab-initio total energy calculations for metals and semiconductors using a plane-wave basis set. *Comput. Mater. Sci.* **6**, 15-50 (1996).

[21] Kresse, G.; Furthmüller, J. Efficient iterative schemes for ab initio total-energy calculations using a plane-wave basis set. *Phys. Rev. B* **54**, 11169-11186 (1996).

[22] Blöchl, P. E. Projector augmented-wave method. *Phys. Rev. B* **50**, 17953-17979 (1994).

[23] Kresse, G.; Joubert, D. From ultrasoft pseudopotentials to the projector augmented-wave method. *Phys. Rev. B* **59**, 1758-1775 (1999).

[24] Dion, M.; Rydberg, H.; Schröder, E.; Langreth, D. C.; Lundqvist, B. I. Van der Waals density functional for general geometries. *Phys. Rev. Lett*. **92**, 246401 (2004).

[25] Kang, S. D.; Snyder, G. J. Transport property analysis method for thermoelectric materials: material quality factor and the effective mass model. Chapter VI in Zevalkink, A.; Kang, S. D.; Snyder, G. J.; Toberer, E. S.; et al. A practical field guide to thermoelectrics: Fundamentals, synthesis, and characterization. *Appl. Phys. Rev.* **5**, 021303 (2018).

[26] Fonari, A.; Sutton, C. Effective Mass Calculator (2012).

[27] Hamberg, I.; Granqvist, C. G.; Berggren, K. -F.; Sernelius, B. E.; Engström, L. Band-gap widening in heavily Sn-doped In_2O_3. *Phys. Rev. B* **30**, 3240 (1984).

[28] Jain, S. C.; McGregor, J. M.; Roulston, D. J. Band-gap narrowing in novel III-V semiconductors. *J. Appl. Phys.* **68**, 3747 (1990).

[29] Snyder, G. J.; Toberer, E. S. Complex thermoelectric materials. *Nat. Mater.* **7**, 106-114 (2008).

[30] Seeger, K. Relaxation times in semiconductors. In *Electronic materials* (Eds. Hannay, N. B.; Colombo, U.) 107 - 126 (Plenum Press, 1973).

[31] Jacoboni, C.; Nava, F.; Canali, C.; Ottaviani, G. Electron drift velocity and diffusivity in germanium. *Phys. Rev. B* **24**, 1014-1026 (1981).

[32] Ichihashi, F.; Kawaguchi, T.; Dong, X.; Kuwahara, M.; Ito, T.; Harada, S.; Tagawa, M.; Ujihara, T. Temperature dependence of carrier relaxation time in gallium phosphide evaluated by photoemission measurements. *AIP Advances* **7**, 115314-6 (2017).

[33] Mir, S. H. Exploring the electronic, charge transport and lattice dynamic properties of two-dimensional phosphorene. *Physica B* **572**, 88−93 (2019).

[34] Yadav, V. K.; Mir, S. H.; Singh, J. K. A computational study of structural, electronic and carrier mobility of boron and phosphorus/nitrogen co-doped graphene. *Physica B* **571**, 291−295 (2019).

[35] Agne, M. T.; Hanus, R.; Snyder, G. J. Minimum thermal conductivity in the context of *diffuson*-mediated thermal transport. *Energy Environ. Sci.* **11**, 609-616 (2018).
[36] Togo, A.; Chaput, I.; Tanaka, I. Distributions of phonon lifetimes in Brillouin zones. *Phys. Rev. B* **91**, 094306 (2015).
[37] Allen, P. B.; Feldman, J. L. Thermal conductivity of glasses: Theory and application to amorphous Si. *Phys. Rev. Lett.* **62**, 645 (1989).
[38] Allen, P. B.; Feldman, J. L.; Fabian, J.; Wooten, F. Diffusons, locons and propagons: Character of atomic vibrations in amorphous Si, *Philos. Mag. B* **79**, 1715–1731 (1999).
[39] Feldman, J. L.; Allen, P. B.; Bickham, S. R. Numerical study of low-frequency vibrations in amorphous silicon, *Phys. Rev. B* **59**, 3551 (1999).
[40] Togo, A.; Tanaka, I. First principles phonon calculations in materials science. *Scr. Mater.* **108**, 1-5 (2015).
[41] Weldert, K. S.; Zeier, W. G.; Day, T. W.; Panthöfer, M.; Snyder, G. J.; Tremel, W. J. Thermoelectric transport in Cu_7PSe_6 with high copper ionic mobility. *J. Am. Chem. Soc.* **136**, 12035−12040 (2014).
[42] Ziman, J. M. Electrons and Phonons: The Theory of Transport Phenomena in Solids (Oxford University Press, 2001).
[43] Róg, T.; Murzyn, K.; Hinsen, K.; Kneller, G.R. *n*Moldyn: A program package for a neutron scattering oriented analysis of molecular dynamics simulations. *J. Comput Chem.* **24**, 657-667 (2003).

Author contributions

B. A. performed calculations by using all declared computational packages and wrote the manuscript. He is the corresponding author of the paper.

I. E. B. took part in the synthesis of Cu_7PS_6 samples, studying their crystallographic properties, and preparation of the cif-file of its symmetry and atomic positions. He took part in the discussion of results presented in the manuscript.

I. P. S. took part in the study of crystallographic properties of Cu7PS6 and measured the corresponding optical bandgap Eg. He took part in the discussion of results presented in the manuscript.

A. I. K. performed calculations of the electron effective mass by using the Effective Mass Calculator and wrote the corresponding part of the manuscript.

M. P. has formulated the main idea of the present paper, he took part in the discussion of all results obtained and wrote the manuscript.

Additional Information (including a Competing Interests Statement)

The authors declare no competing interests.

Figure legends

Fig. 1. Band structure (a) and partial density of states (b) of Cu_7PS_6 for the symmetry space group no. 198 at the points Γ - 000, X – 010, M – ½½0, R - ½½½, X1 – 100 of BZ. The highest energy of the top valence band is placed at $E = 0$ eV. In inset, the enlarge $E(k)$ dependence of the top valence band v236 in the vicinity of Γ-point, shown by arrow

Fig. 2. (a) Fermi level shift ΔE_F as function of the excess electron/hole concentration $n^{2/3}$ for Cu_7PS_6. Negative values of $n^{2/3}$ correspond to the excess electrons (n-type Cu_7PS_6) and positive ones to the excess holes (p-type Cu_7PS_6). Signs of the effective masses $m^* = 0.581\ m_e$ and $m^* = -6.15\ m_e$ are chosen to be compatible with the effective mass definition $m^* = \hbar^2/(d^2E/dk^2)$; (b) Effective electron mass m^*/m_e as function of the excess electron/hole concentration n calculated from BoltzTraP2 Seebeck coefficient α and relation (1) (dashed line) and from the data of Fig. 2a (solid line)

Fig. 3. Dependences of (a) Seebeck coefficient α and (b) carrier relaxation time τ on carrier concentration n for Cu_7PS_6 at the temperatures 300 K, 400 K, and 490 K

Fig. 4. Dependences of (a) electric conductivity σ, (b) power factor *PF*, and figure of merit *ZT* on carrier concentration *n* for Cu_7PS_6 at the temperatures 300 K, 400 K, and 490 K

Fig. 5. Dependences of (a) coefficient of electron thermal conductivity κ_e and (b) figure of merit *ZT* on carrier concentration *n* for Cu_7PS_6 at the temperatures 300 K, 400 K, and 490 K. The values *ZT* correspond to the coefficient of thermal conductivity κ = 0.7 W/(m·K)

Fig. 6. Temperature dependences of lattice thermal conductivity coefficient $\kappa_{ph}^{(1)}$ of Cu_7PS_6 obtained using Phono3py with displacement amplitude of 0.3 Å and *q*-meshes of 3×3×3 (dashed line) and 6×6×6 (solid line)

Fig. 7. Temperature dependence of lattice thermal conductivity coefficient $\kappa_{ph}^{(2)}$ of Cu_7PS_6 obtained by using the results of molecular dynamics calculations and relation (7)

Supplementary Files

This is a list of supplementary files associated with this preprint. Click to download.

- SICu7PS6SR1872021.docx